The current issue and full text archive of this journal is available at
www.emeraldinsight.com/0961-5539.htm

Received 11 January 2008
Revised 15 April 2008
Accepted 30 April 2008

Numerical and experimental approach to cavitation surge obstruction in water pump

Ignacijo Biluš and Andrej Predin
Faculty of Mechanical Engineering, University of Maribor, Maribor, Slovenia

Abstract

Purpose – This study aims to present the analysis of methods for cavitaion surge obstruction in water pump systems with particular focus on the two different inlet geometry configurations.
Design/methodology/approach – A cavitating flow field was simulated by RANS based computational fluid dynamics (CFD) program for different pump configurations operating in the unstable cavitation regime, inducing surging process. Numerical simulation results were compared to visualization and measurements results.
Findings – Presented results show that a hydro dynamically induced surging regime could be limited and further advantages regarding operating characteristics of radial pumps could be achieved with presented geometry modifications.
Originality/value – This study provides insight into complicated transient cavitation flow patterns in conventional centrifugal pumps and introduces effective geometry optimization ideas useful to researchers and engineers in the area of fluid dynamics and hydromachinery.
Keywords Cavitation, Pumps, Liquid flow, Fluid dynamics
Paper type Research paper

Nomenclature

R_B	bubble radius
p_v	pressure in the bubble
p	ressure in the surrounding liquid
ρ_f	liquid density
ρ_g	vapor density
σ	surface tension between the liquid and vapor
V_B	bubble volume
m_B	bubble mass
t	time
N_B	bubble number density
r_g	volume fraction
$\dot{m}_{fg}$	interphase mass transfer per unit volume
F	empirical factor
r_{nuc}	volume fraction of nucleation sites
V	physical volume
V'	volume available to flow
γ	volume porosity at a point
$\mathbf{A}'$	vector area available to flow
$\mathbf{A}$	infinitesimal planar control surface of vector area
$\mathbf{K}$	isotropic porosity tensor
S	production and dissipation terms
$\mathbf{U}$	actual fluid velocity vector
μ_e	effective viscosity (laminar or a turbulent)
$\mathbf{R}$	resistance to flow in the porous medium

International Journal of Numerical Methods for Heat & Fluid Flow
Vol. 19 No. 7, 2009
pp. 818-834
© Emerald Group Publishing Limited
0961-5539
DOI 10.1108/09615530910984091

Introduction

The trend toward higher speed and power in order to achieve high performance characteristics has inevitably increased the potential for operating instabilities of modern pumps. Even in the absence of cavitation and its complications, these phenomena can lead to performance loss and in worst condition to structural failure.

One of the major sources of instability in a centrifugal pump is, as mentioned, cavitation within the pump. Cavitation of a centrifugal pump is the result of insufficient net positive suction head and can occur within the entire range of operating conditions. Cavitation may cause three different and undesirable effects:

(1) a drop in head and efficiency curves;

(2) damage to the impeller by pitting and erosion; and

(3) structure vibration (Bergant, 2000) and resulting noise (Čudina, 2006). Therefore, the cavitation process must be prevented by all means.

A lot of research works regarding flow induced noise in centrifugal pumps (Langhtjem and Olhoff, 2004) and flow induced vibrations exist in literature. Owing to complex nature of noise and vibration phenomena, it is not easy to quantitatively evaluate (Jiang *et al.*, 2007) the contribution of secondary flow effects and cavitation on system. According to this, the purpose of present study is the general CFD investigation of the generic problem of turbulent flow through the rotating pump impeller, validation of computational procedure to the available experiments and confirmation of cavitation obstruction methods effect.

In case of cavitating flow regimes, three distinct operating possibilities are known:

(1) the stable regime, where the majority of cavitating centrifugal pumps operate;

(2) unstable regime described as hydro dynamically induced cavitation surging; and

(3) transient regime, described as thermodynamically induced surging Grist (1998).

The numerical simulation was used for analysis of the influences of simple motionless four blade guiding device and porous blade inlet on cavitating characteristics of radial pump in unstable cavitating regime, where cavities grow in a region near the inlet blade tip before being folded back into the backflow. The low pressure gradients within this backflow recirculation enable them to grow rapidly for considerable distances.

Cavitation surging

Reducing the flowrate passing through a centrifugal pump gives rise to the possibility of three distinct flow regimes. The most important is stable regime and this is where nearly all pumps operate. If either a pump or the adjacent plant is incorrectly designed or maloperated the other regimes may be encountered.

In the transient regime little or no volumetric flow interchange occurs between fluid in or near impeller and the liquid in surrounding pipework. According to this, practically all the energy put into the fluid goes to overcome hydraulic churning losses and this result in temperature rise. If the volumetric expansion is constrained the inlet temperature pressure builds up and the process associated with cavity growth and collapse is dominated by the thermodynamically induced changes.

Hydro dynamically induced cavitation surging

Hydro dynamically induced surging or unstable operating regime can occur at low (off-design) values of capacity in almost all centrifugal pumps. The onset and intensity of cavitation surging is primarily determined by the shape of the impeller blades at impeller inlet. The extent to which cavities travel away from the impeller is determined by inlet pipe geometry. In most impeller-pipe configurations the low pressure regions are localized and backflow recirculation area giving raise to cavitation surging hardly leaves the inlet blade region. On the other hand, the prerotating flow pattern in inlet pipe with extension to cavitation process and connected to large curvature of streamlines in region, still presents a pretentious problem of computational fluid mechanics.

Flow guiding device as a tool for cavitation obstruction

In some pumps, particularly those for which the inlet pipe has axial symmetry with impeller eye, the associated backflow extends well into the inlet pipe. It is known, that in pumps, where a backflow recirculation device (Figure 1) is fitted, the intensity and extent of surging is much reduced over a wide flowrate range.

Another known powerful method to improve the cavitation performance is the attachment of an inducer just upstream of the main impeller Kimura *et al.* (2006) and many researchers all over the world study different pump inducer geometry versions in order to achieve reliable and cavitation free operating characteristics Kim *et al.* (2006).

According to relative complicated "pipe in pipe" construction of backflow recirculation system and regarding to pump inducer price, the simplified flow guiding device shown in Figure 1(b) was introduced and analysed.

Geometry of physical model

Simple copper made cross in form of four guiding blades with inclination angle $\alpha = 20^{\circ}$ was put into the transparent pipe at the impeller entrance. Guiding blades length was equal $l = 1.15D$, where D present the inlet pipe diameter.

Described flow guiding pipe system was connected to the conventional closed loop pump testing installation as shown in Figure 2.

For experimental test purposes, commercial radial water pump with design speed 2900 rpm, maximal capacity $Q_{max} = 0.027\,m^3/s$ and maximal head $H_{max} = 25\,m$ was used. Operating characteristics of the pump are evident from Figure 3(a).

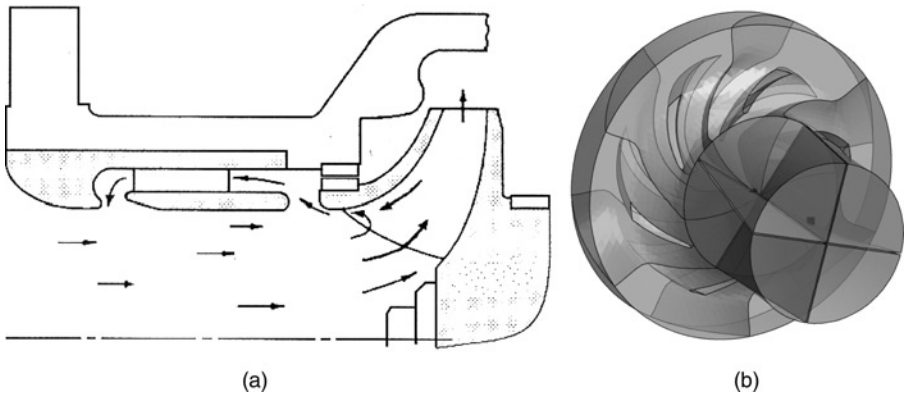

Figure 1.
Backflow recirculation system (a) and simple axial flow guiding device in front of centrifugal impeller (b)

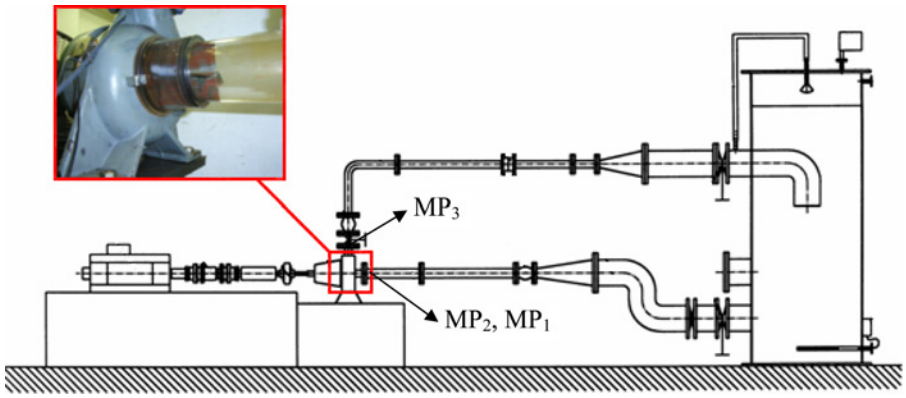

Figure 2.
Measuring system drawing

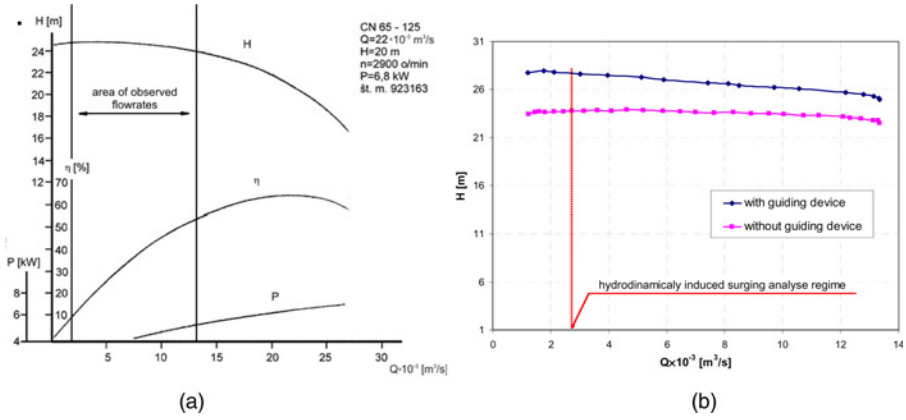

Figure 3.
Operating characteristics of tested pump (a) and measured influence of guiding device on pump head (b)

It is evident from Figure 3(b) that measured pressure difference curve agrees with operating characteristic defined by the pump manufacturer Figure 3(a) in the case of conventional inlet pipe geometry. On the other side, it is also evident that guiding vanes device increases the achieved pressure difference at the flowrates up to $Q = 0.5Q_{max}$. The reason for this could be found in better flow attack angles at the pump inlet.

Measurement system

For the operating characteristics and frequency analysis the measuring equipment shown at Figure 4 was used.

Guiding device vs cavitation surge pressure pulsations

Pressure pulsations connected to cavitation surging were measured at the two different measuring points (MP_2, MP_1) placed in the upstream direction of radial pump entrance pipe as shown in Figure 2. Absolute piezo-resistive pressure transducers KELLER with pressure range up to 2 and up to 10 bar (FS) with frequency response 20kHz were connected to A/D measuring equipment. Pressure pulsations were analysed at flowrate equal to 12 percent of flowrate at best efficiency point (Q_{BEP}).

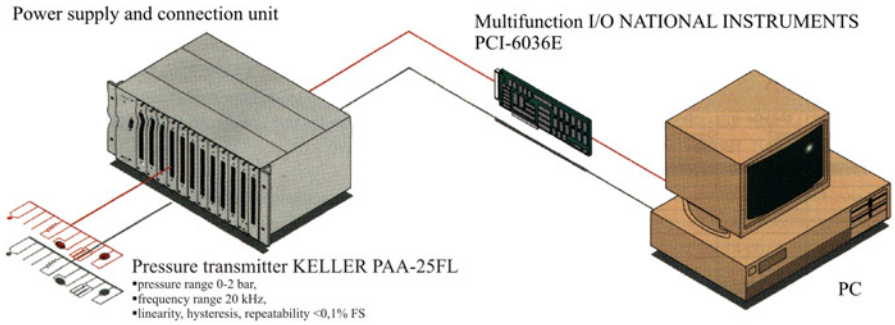

Figure 4.
Measurement system

Measurements results

A frequency analysis with fast Fourier transformation (FFT) was made and same operating regime was set for the example with and without guiding device. Frequency analyses results records are shown in plots at Figures 5 and 6.

It is evident from frequency analyses presented in Figure 5, that guiding blades reduce the amplitudes at whole frequency range. This amplitude chocking is especially strong at rotating impeller basic frequency $f_{imp} \approx 50$ Hz, its harmonics and blade passing frequency $f_{blade} \approx 300$ Hz with its sub-harmonic.

These results confirm other authors analyses defining the super synchronous speeds of rotating cavitation with range up to 1.4 comparing to impeller rotating speed Brennen (1994).

Following the relative strong pressure pulsations at distance equal to five pipe diameters (5*D*) from impeller entrance eye, second measurement series were done at position MP_2 corresponding to distance equal to three inlet pipe diameters (3*D*).

From the presented FFT analyse of pressure pulsations at MP_2 could be concluded that the guiding device reduces pressure pulsation amplitudes of characteristic frequencies and hydro dynamically induced surge pulsations with lower frequencies Bergant (2000).

Numerical simulation

Owing to fast computer capabilities increase and according to intensive experimental methods development, optimization of rotating Matijašević *et al.* (2002) and cavitating Dular *et al.* (2007) hydraulic machinery became possible in the past. In last years CFD also matured as a useful tool in the search for optimal solutions regarding performance and flow behaviour, Marjavaara and Lundström, (2007). This section presents the approach to numerical simulation of strongly swirling multiphase flow at different geometries of cavitating pump inlet.

Since the measurement results have shown the high pressure oscillations and therefore strongly fluctuating flowrate, further adjustment of conventional eddy viscosity turbulence model should be done in order to simulate the phenomena properly. A difficulty associated with solving such swirling flows is that the eddy viscosity model fails to capture the anisotropy of strain and Reynolds stresses under the action of centrifugal and Coriolis forces. According to this, it is recommended to employ advanced turbulence model or to systematic adjust the standard k-ε(or k-ω) model constants. Wang *et al.* (2006) find the RSM model; despite to the fact of providing the information of all stresses components and containing the exact terms of swirling effect in its stress transport equations, not recommendable. The reason for this could be

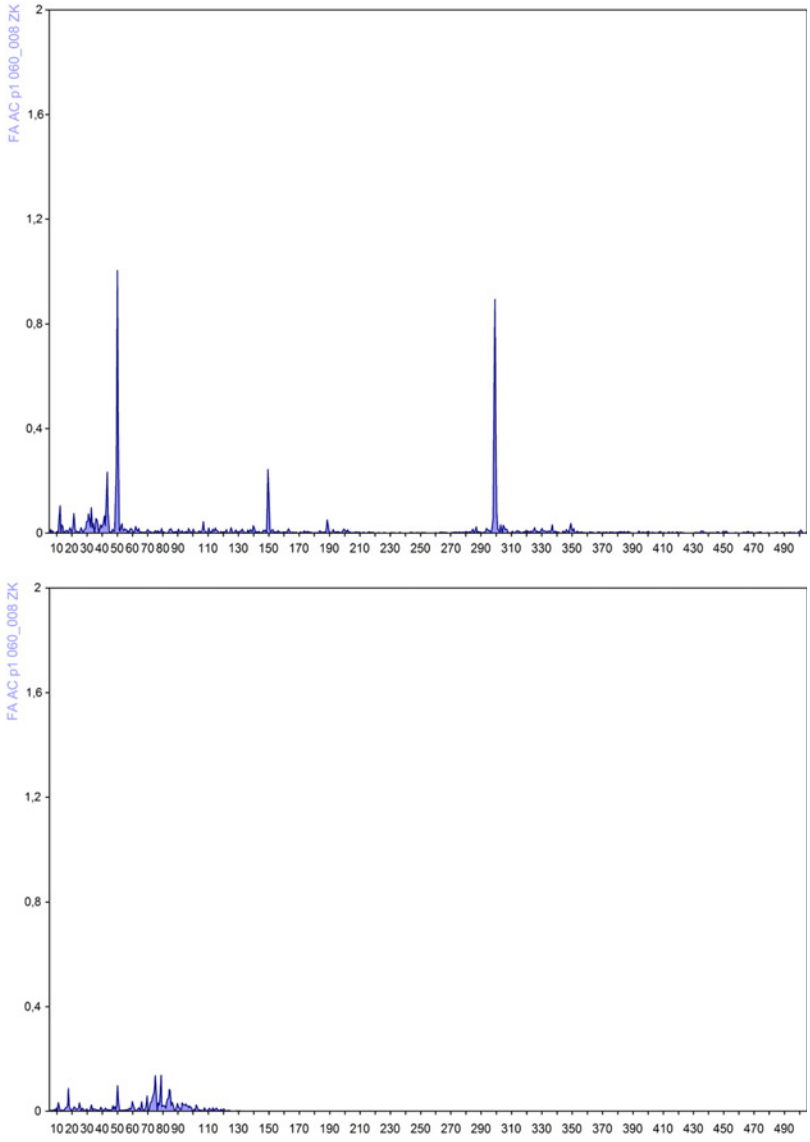

Figure 5.
Pressure pulsations at MP_1 without guiding blades (a) and with guiding blades (b)

in fact that for high swirl rate the RSM is still not sufficient to account for the anisotropies of the dissipation and strain. On the other hand, Benim *et al.* (2007) find the best agreement of the numerical simulation and experiment in the case of turbulent jet impinging onto rotating disc with k-ω model. Matijašević *et al.* (2006) analysed the effect of turbulence model on unsteady fluid flow in radial fan and concluded strong results dependency on applied mathematical model and other influential factors.

Considering the two-phase flow, there exist numerical difficulties relating to the strong coupling between the pressure field and the void ratio and to the coexistence of strong compressibility of the two-phase medium with the quasi incompressible

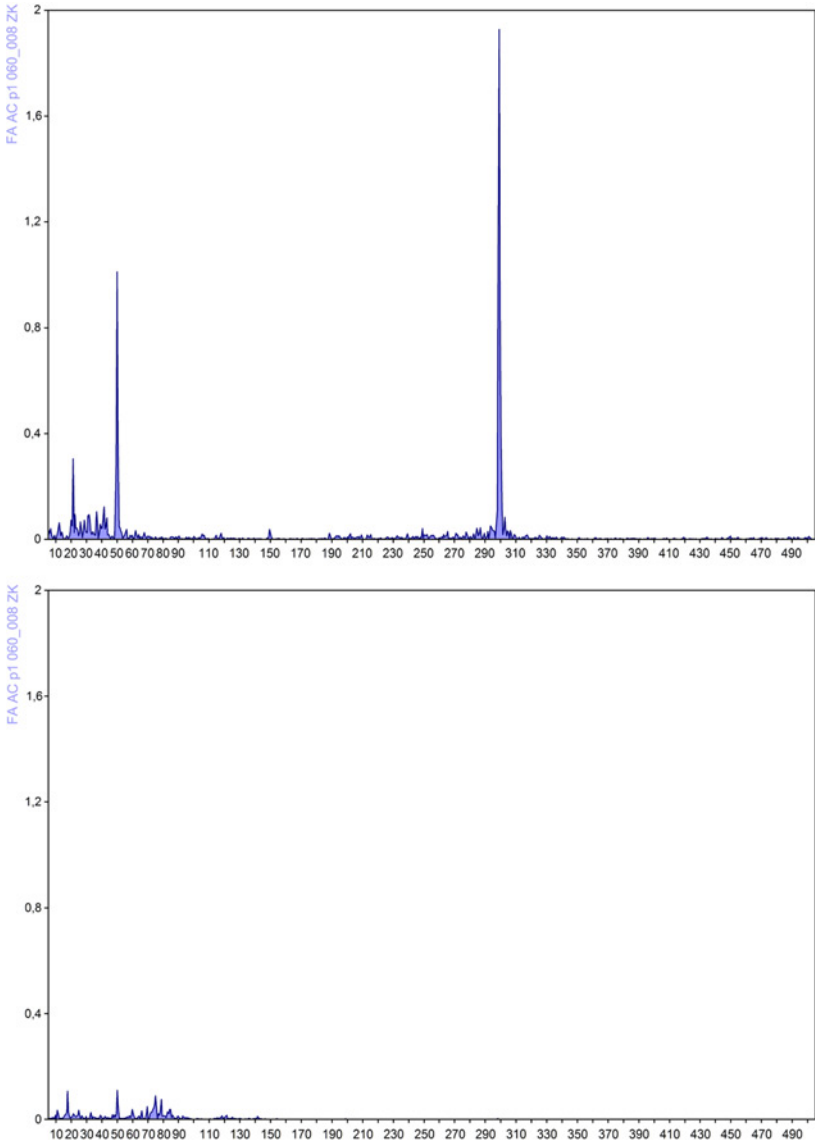

Figure 6.
Pressure pulsations at MP_2 without guiding blades (a) and with guiding blades (b)

behaviour of the pure liquid flow. Moreover, the influence of the turbulence on unsteady two-phase compressible flows is not yet well known. Coutier-Delgosha *et al.* (2003) introduced and verified the modified k-ε model with mixture turbulent viscosity correction in the low void ratio areas, for the example of Ventury type section.

The turbulence in present work is modelled with standard k-ε model and by usage of scalable wall functions. Although this model is unable to reproduce all details of the flow accurately, it was chosen since there are not known improved and verified turbulence model dealing with rotating swirling two-phase flows in open literature.

Computational mesh and boundary conditions

For presented simulation, unstructured tetrahedral mesh, shown in Figure 7, was used. At the pipe inlet, mass flow was prescribed and opening boundary condition with relative static pressure was defined at the impeller exit diameter.

At the rotating and stationary mesh interface, the frozen rotor and transient rotor stator model was prescribed, respectively.

For the porous blade region, the isotropic loss model was applied and permeability value was set to 10^{-15} m^2. According to small blade width, this value was constant during analysis.

Mathematical model

Considering the homogeneous two-phase flow, common flow field and other relevant fields such as temperature and turbulence are shared by both fluids (water and water vapor). This allows some simplifications to be made to the multi-fluid model. For a given transport process, the homogeneous model assumes that the transport quantities (with the exception of volume fraction) for that process are the same for both phases.

Homogeneous two-phase transport model included in commercial software ANSYS-CFX was used for surging simulation.

For this work, the discretization of pressure gradient term and diffusion term are obtained with shape functions while the discretization of advection term is done with high resolution scheme.

The Rayleigh-Plesset model is implemented in the multiphase framework as an interphase mass transfer model in used numerical code. The Rayleigh-Plesset equation provides the basis for the rate equation controlling vapor generation and condensation. The Rayleigh-Plesset equation describing the growth of a gas bubble in a liquid is given by

$$R_B = \frac{d^2R_B}{dt^2} + \frac{3}{2}\left(\frac{dR_B}{dt}\right)^2 + \frac{2\sigma}{\rho_f R_B} = \frac{p_v - p}{\rho_f} \tag{1}$$

where R_B represents the bubble radius, p_v is the pressure in the bubble (assumed to be the vapor pressure at the liquid temperature), p is the pressure in the liquid surrounding the bubble, ρ_f is the liquid density, and σ is the surface tension coefficient between the liquid and vapor. Note that this is derived from a mechanical balance, assuming no thermal barriers to bubble growth. Neglecting the second order terms (which is appropriate for low oscillation frequencies) and the surface tension, this

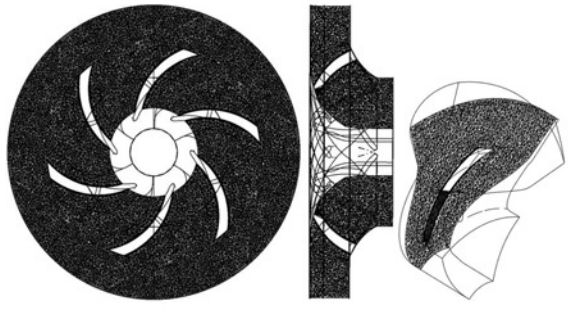

Geometry	Number of elements
impeller	965.460
inlet pipe	123.139
porous blades	146.964
TOTAL	**1.235.563**

Figure 7.
Computational mesh details

equation reduces to

$$\frac{dR_B}{dt} = \sqrt{\frac{2}{3}\frac{p_v - p}{\rho_f}} \tag{2}$$

The rate of change of bubble volume follows as

$$\frac{dV_B}{dt} = \frac{d}{dt}\left(\frac{4}{3}\pi v R_B^3\right) = 4\pi R_B^2 \sqrt{\frac{2}{3}\frac{p_v - p}{\rho_f}} \tag{3}$$

and the rate of change of bubble mass is

$$\frac{dm_B}{dt} = \rho_g \frac{dV_B}{dt} = 4\pi R_B^2 \rho_g \sqrt{\frac{2}{3}\frac{p_v - p}{\rho_f}} \tag{4}$$

If there are N_B bubbles per unit volume, the volume fraction r_g may be expressed as

$$r_g = V_B N_B = \frac{4}{3}\pi R_B^3 N_B \tag{5}$$

and the total interphase mass transfer rate per unit volume is

$$\dot{m}_{fg} = N_B \frac{dm_B}{dt} = \frac{3 r_g \rho_g}{R_B} \sqrt{\frac{2}{3}\frac{p_v - p}{\rho_f}} \tag{6}$$

This expression has been derived assuming bubble growth (vaporization). It can be generalized to include condensation as follows:

$$\dot{m}_{fg} = F \frac{3 r_g \rho_g}{R_B} \sqrt{\frac{2}{3}\frac{|p_v - p|}{\rho_f}} \mathrm{sgn}(p_v - p) \tag{7}$$

where F is an empirical factor which may differ for condensation and vaporization, designed to account for the fact that they may occur at different rates (condensation is usually much slower than vaporization).

Despite the fact that upper equation has been generalized for vaporization and condensation, it requires further modification in the case of vaporization.

Vaporization is initiated at nucleation sites (most commonly non-condensable gases). As the vapor volume fraction increases, the nucleation site density must decrease accordingly, since there is less liquid. For vaporization, r_g is replaced by $r_{nuc}(1 - r_g)$ to give

$$\dot{m}_{fg} = F \frac{3 r_{nuc}(1 - r_g) \rho_g}{R_B} \sqrt{\frac{2}{3}\frac{|p_v - p|}{\rho_f}} \mathrm{sgn}(p_v - p) \tag{8}$$

where r_{nuc} is the volume fraction of the nucleation sites. Source equation is maintained in the case of condensation. It is important to note that in this model R_B represents the radius of the nucleation sites.

To obtain an interphase mass transfer rate, further assumptions regarding the bubble concentration and radius are required. The Rayleigh-Plesset cavitation model implemented in ANSYS CFX uses the following defaults for the model parameters:

$$R_B = 1\,\mu\text{m}, \quad r_{nuc} = 5 \times 10^{-4}, \quad F_{vap} = 50, \quad F_{cond} = 0.01.$$

CFD results

The present chapter includes results comparison for both inlet pipe geometries (with and without guiding device). Diagrams and photographs are showing same operating regime regarding relative pressure in the water reservoir (NPSH value) and convection term (flowrate) height. The influence of geometry on cavitation swirl has been analysed with stress laid on two-phase area propagation.

Since we have to model a change in a reference frame between the rotating domain (impeller) and stationary domain (pipe), the transient fluid-fluid interface has been defined.

Figure 8 shows operating regime pattern for system operating out of design point – with reduced flowrate for both geometries.

Strong prerotating motion Predin and Biluš (2003) in the inlet pipe especially near pipe walls is evident from the Figure 8(a) showing the case of geometry without guiding device.

Comparing to the streamlines plot at Figure 8(b) it could be concluded, that guiding device stops general swirling flow and splits it into four smaller flow channels where smaller swirls occur.

Figure 9 shows the unstable cavitating operating regime with a strong recirculating cloud of vapor bubbles at the inlet pipe walls connected to cavitation number decrease.

Strong recirculatory motion with an active flow area in the middle of the pump is shown in the picture showing geometry without guiding device (a). It is obvious from water vapor isosurface that cavitation swirl takes place in the low pressure region of the prerotating active flow area.

Splitted recirculation cloud is evident from Figure 9(b) showing operating regime with guiding device. It is evident, that cavitation cloud remains in the guiding device channels.

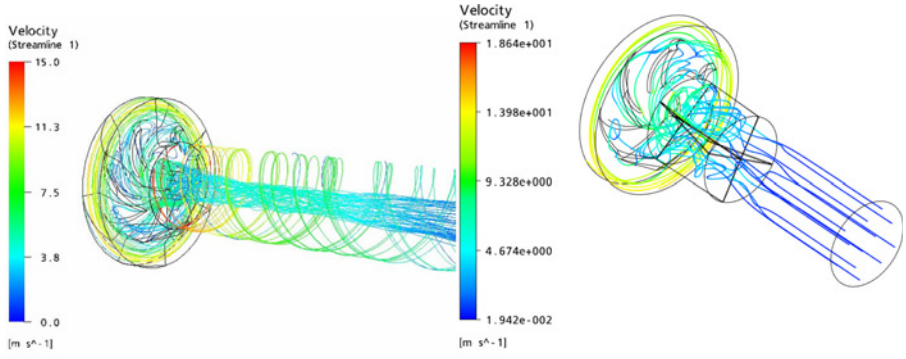

Figure 8.
Operating regime visualization using streamlines plots for both analysed geometries

Figures 10 and 11 show the cavitation visualization comparison at both geometries.

It can be concluded from Figures 10 and 11 that guiding vanes split the rotating two-phase region into the four flow passages. Evident is that the cavitation region becomes shorter. The reason for this could be in new non-prerotating flow regime, which prevent the diffusion driven extension of cavitation from impeller to suction pipe and new static vs dynamic pressure balance.

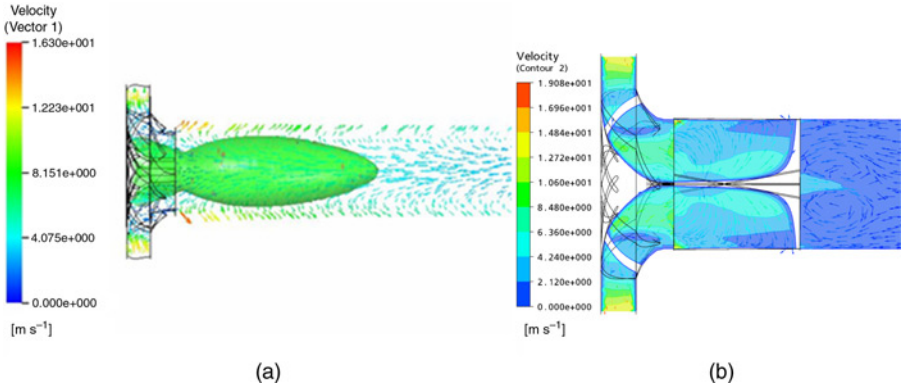

Figure 9.
Unstable cavitating pump operating regime without (a) and with guiding device (b)

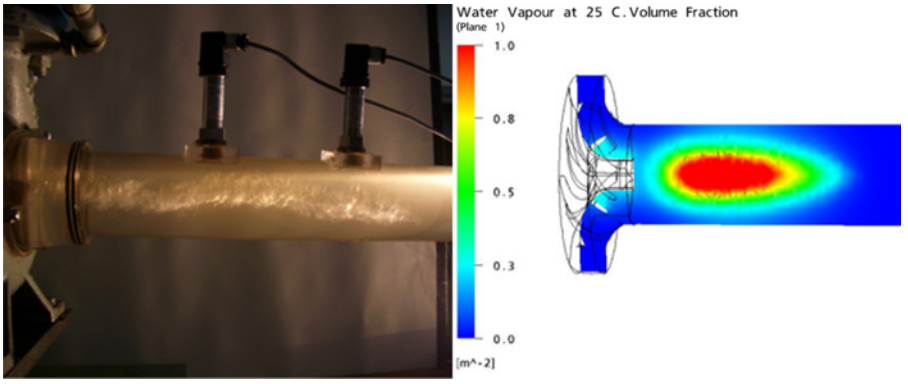

Figure 10.
Hydro dynamically induced cavitation surging on the inlet geometry without guiding device

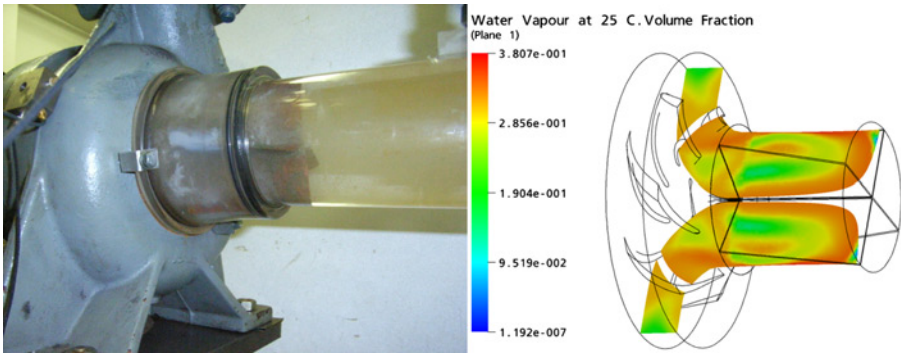

Figure 11.
Hydro dynamically induced cavitation surging on inlet geometry with guiding device

There is a good agreement evident from comparison of results. According to this, we can conclude, that the homogenous cavitation transport model, used in study, which is based on the Raleigh–Plesset equation (inter phase mass transfer), presents as effective tool for prediction of cavitation in hydraulic machinery.

Porous impeller blades inlet region and cavitation surging

Secondary flow and vorticity as a cavitation drift

In general, the flow entering the blade row is nonuniform. The radial gradient in velocity and stagnation pressure may be caused by casing/hub wall boundary layers or by the presence of an upstream blade row.

In order to explain the mechanism of vorticity appearance, let us consider two dimensional cascade blade row and inlet velocity profile. It is known that the streamline in a cascade in the uniform flow region deflects from the streamline in the shear layer. If we neglect viscous effects and the velocity variation in the n (normal) direction and assume the flow to be incompressible and steady, the pressure gradient in normal direction is balanced by the centripetal acceleration along the streamline.

Hence

$$\left(\frac{\partial p}{\partial n}\right)_A = \frac{\rho u_A^2}{R_A}$$

where R_A is the radius of the streamline at point A, where the total streamwise velocity is u_A.

If the boundary layer approximation is invoked, the pressure gradient normal to the side wall for the streamlines in the uniform flow region and viscous layer would be the same, and thus we obtain

$$\left(\frac{\partial p}{\partial n}\right)_A = \left(\frac{\partial p}{\partial n}\right)_B = \frac{\rho u_A^2}{R_A} > \frac{\rho u_B^2}{R_B}$$

Because $u_B < u_A$ and $R_B = R_A$, there is an imbalance between the normal pressure gradient and the centripetal acceleration and thus streamline in the shear layer will deflect more, developing a cross flow and causing pressure oscillation in blade row.

This simple mechanism provides a clear physical reasoning for the occurrence of the secondary vortices may (with certain pressure decrease) lead to cavitation inception in blade row. Since the secondary flow is thus generated whenever a shear layer or normal vorticity is turned through cascade, the idea of porous blade at inlet raised. In order to achieve the boundary effect decrease and to allow the cross flow to pass through blades in predefined region, they were divided according to Figure 12.

Mathematical model for flow simulation in porous regions

The mathematical model for flow simulation in porous regions is at once both a generalization of the Navier-Stokes equations and of Darcy's law commonly used for flows in porous regions. The model retains both advection and diffusion terms.

In deriving the continuum equations, it is assumed that "infinitesimal" control volumes and surfaces are large relative to the interstitial spacing of the porous medium, though small relative to the scales that have to be resolved. Thus, given control cells and control surfaces are assumed to contain both solid and fluid regions.

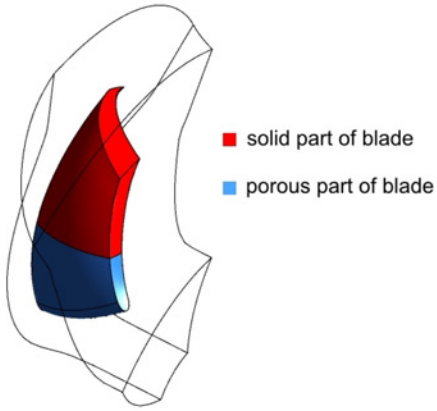

Figure 12.
Geometry of porous blade

The volume porosity γ at a point is the ratio of the volume V' available to flow in an infinitesimal control cell surrounding the point, and the physical volume V of the cell. Hence

$$V' = \gamma\, V$$

It is assumed that the vector area available to flow, $\mathbf{A}'$, through an infinitesimal planar control surface of vector area $\mathbf{A}$ is given by

$$\mathbf{A}' = \mathbf{K} \cdot \mathbf{A}$$

where $\mathbf{K} = \left(K^{ij}\right)$ is the area porosity tensor. Ansys CFX used for numerical simulation in present version only allows $\mathbf{K}$ to be isotropic.

The general scalar advection-diffusion equation in a porous medium becomes

$$\frac{\partial}{\partial t}(\gamma\rho\phi) + \nabla \cdot (\rho\mathbf{K} \cdot \mathbf{U}\phi) - \nabla \cdot (\Gamma\mathbf{K} \cdot \nabla\phi) = \gamma S$$

In addition to the usual production and dissipation terms, the source term S will contain transfer terms from the fluid to the solid parts of the porous medium.

In particular, the equations for conservation of mass and momentum are

$$\frac{\partial}{\partial t}\gamma\rho + \nabla \cdot (\rho\mathbf{K} \cdot \mathbf{U}) = 0$$

and

$$\frac{\partial}{\partial t}(\gamma\rho\mathbf{U}) + \nabla \cdot (\rho(\mathbf{K} \cdot \mathbf{U}) \times \mathbf{U}) - \nabla \cdot \left(\mu_e\mathbf{K} \cdot \left(\nabla\mathbf{U} + (\nabla\mathbf{U})^T\right)\right) = -\gamma\mathbf{R} \cdot \mathbf{U} - \gamma\nabla p$$

where $\mathbf{U}$ is the true velocity, μ_e is the effective viscosity (laminar viscosity or a turbulent quantity) and $\mathbf{R} = \left(R^{ij}\right)$ represents a resistance to flow in the porous medium. This is in general a symmetric positive definite second rank tensor, in order to account for possible anisotropies in the resistance.

In the limit of large resistance, a large adverse pressure gradient must be set up to balance the resistance. In that limit, the two terms on the r.h.s. of momentum equation are both large and of opposite sign, and the convective and diffusive terms on the l.h.s. are negligible. Hence, momentum equation reduces to

$$\mathbf{U} = -\mathbf{R}^{-1} \cdot \nabla p$$

Hence, in the limit of large resistance, we obtain an anisotropic version of Darcy's law, with permeability proportional to the inverse of the resistance tensor. However, unlike Darcy's law, we are working with the actual fluid velocity components **U**, which are discontinuous at discontinuity in porosity, rather than the continuous averaged superficial velocity, $\mathbf{Q} = \mathbf{K} \cdot \mathbf{U}$.

CFD results

The following section presents the numerical simulation results of the pump with porous blades at inlet, operating in cavitation inception regime.

Figure 13 shows the influence of porous blade on calculated pump head characteristic.

It can be concluded form Figure 13 that pump head decreases with porosity. The head drop in the flowrate range of cavitation surging regime (under optimal flowrates) increases from 7 percent (at $0.02 \times Q_{BEP}$) up to 17 percent (at $0.08 \times Q_{BEP}$) comparing to normal un-porous blade.

Since the local pressure fluctuations initiate cavitation inception in blade rows, porosity could decrease the vapor concentrations and two-phase area propagation. According to this, numerical simulation of flow was done for cavitation inception regime and different blade porosity values. The simulation results are shown in Figure 14.

It is evident from Figure 14 that cavitation regions decrease with volume porosity increase. Apart from the fact of lower head, porosity could be used as a cavitation obstruction tool since it reduces destructible potential of phenomena. Comparing to normal blades geometry simulation result, evident in Figure 15, it could be written that both analysed volume porosity values (Figure 14) decrease cavitation region distinctively.

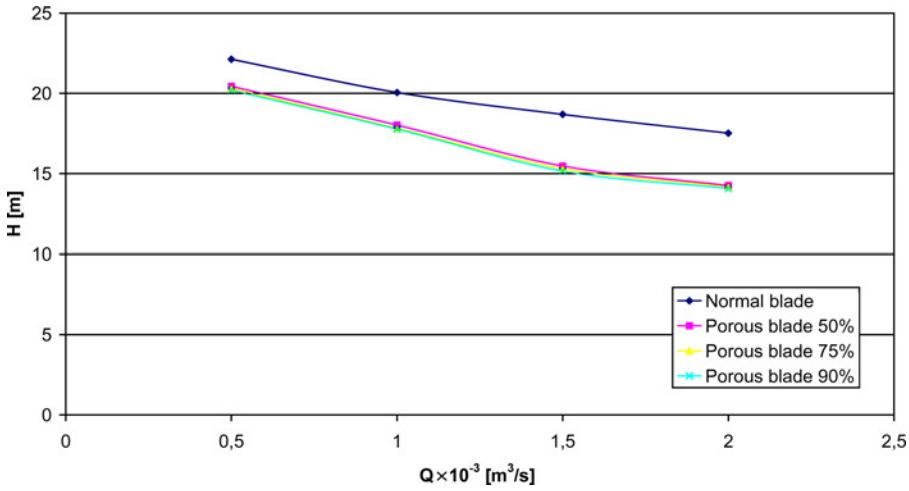

Figure 13.
Porous blade and the pump head

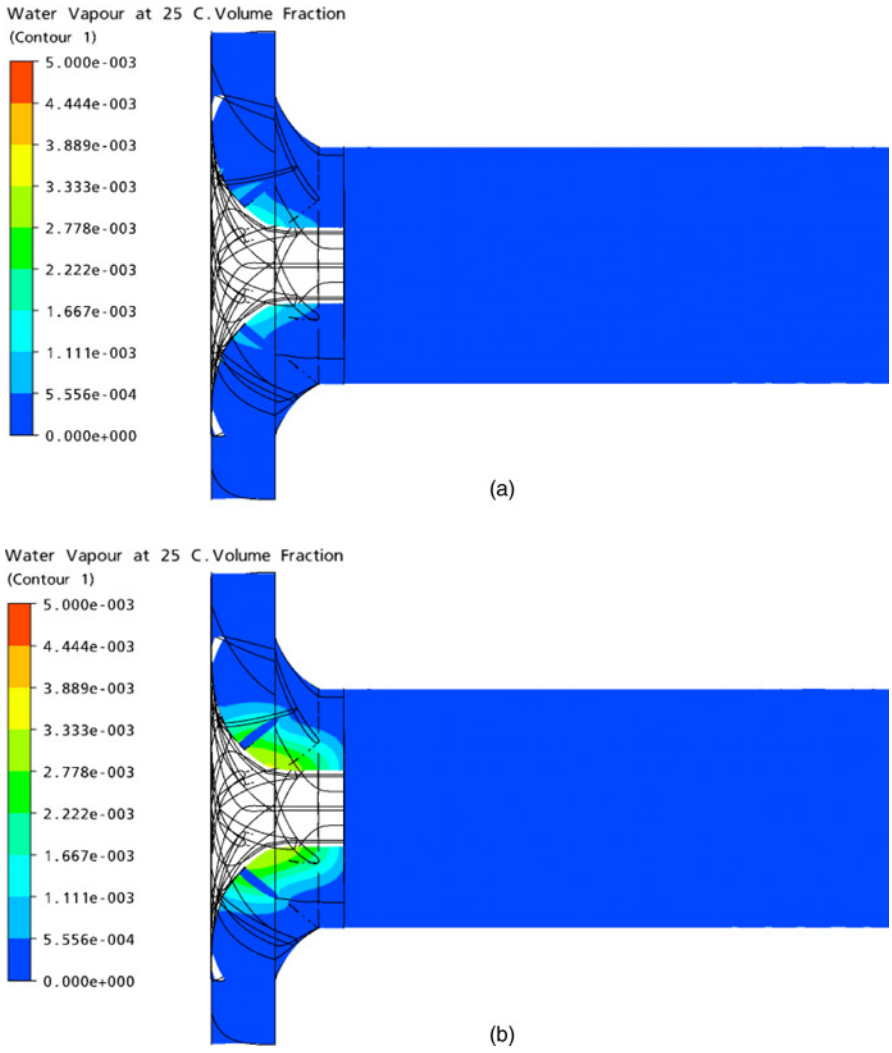

Figure 14.
Cavitation regions in centrifugal pump impeller at 90 percent (a) and 50 percent volume porosity (b)

Conclusions

The present work demonstrates the possibilities and difficulties of using CFD in the optimization process of cavitating pump inlet. The article includes numerical and experimental results for two inlet pipe geometries showing that hydro dynamically induced surge is system instability that involves not just the pump characteristics but those of the complete piping system at complicated unstable operating regime.

Results confirms the mechanism of (diffusion driven) cavitation to originate from pre-existed low pressure regions formed at blade suction sides or even as consequence of oscillations caused with swirling cross flow at in the impeller blade rows.

Results show that use of the simple guiding device improves the cavitation state resulting in dominant cavitation pressure pulsations and two-phase cloud decrease.

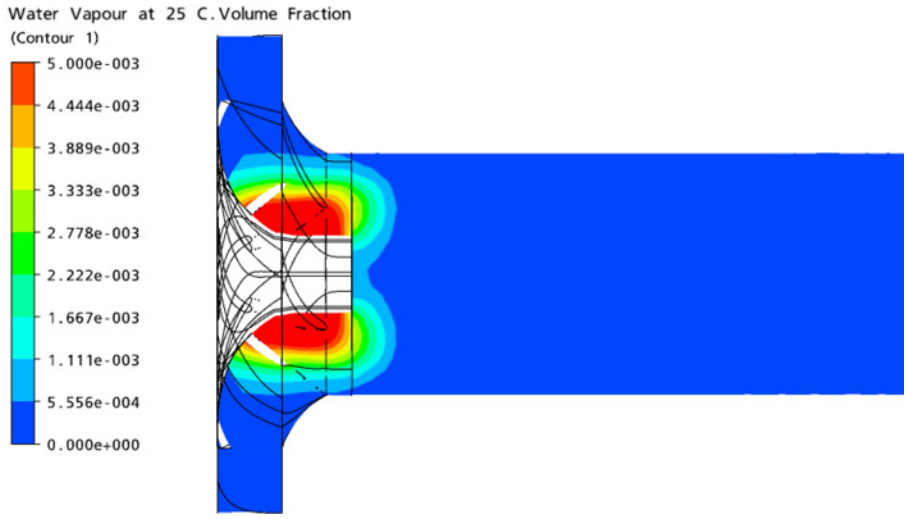

Figure 15.
Cavitation region in centrifugal pump with normal blade

It is evident from the experimental analysis that dominant frequencies scale with the impeller rotating speeds, where some of them show large independency of the impeller rotation frequency at both inlet pipe geometries.

It can be written that used homogenous mathematical model presents suitable tool for prediction of cavitation in turbo machinery and fast method for geometry optimization despite to the mismatch comparing to physics.

The computational fluid mechanics results confirm that the cavitation region transition from the area of impeller channels up in the entrance pipe is connected to recirculation flow and with decreased active flow area in the intake pipe, respectively.

The swirl length is based on the geometry of the pump entrance area and pressure in the reservoir, which defines the volume fraction of the gas phase and the cavitation swirl diameter.

Simple guiding device splits the prerotating flow motion into four disconnected flow channels resulting in operating characteristics increase and possible operating complications connected with pressure pulsations and vibrations decrease.

Porous impeller blades inlet region decreases the cavitation propagation on the one side and decreases the pump head on the other. According to this, user should balance between both effects or use cheaper and simpler guiding device.

The overall result is that CFD, with k-ε approach, is capable of offering satisfactory results in the design process of hydraulic components, but owing to transient nature of complicated swirling turbulent two-phase flow regime in analysed system, both numerical and experimental research methods should be used for similar studies.

References

Benim, A.C., Ozkan, K., Cagan, M. and Gunes, D. (2007), "Computational investigation of turbulent jet impinging onto rotating disc", *International Journal of Numerical Methods for Heat and Fluid Flow*, Vol. 17 No. 3, pp. 284-301.

Bergant, A. (2000), "Transient cavitating flow in piping systems", *Acta Hydrotech*, Vol. 18 No. 29, pp. 5-17.

Brennen, C.E. (1994), *Hydrodynamics of Pumps*, Concepts ETI Inc, USA and Oxford University Press, Oxford.

Coutier-Delgosha, O., Patella, R.T. and Reboud, J.L. (2003), "Evaluatuion of the turbulence model influence on the numerical simulations of unsteady cavitation", *Journal of Fluids Engineering*, Vol. 125 No. 1, pp. 38-45.

Čudina, M. (2006), "Noise as an indicator of cavitation in a centrifugal pump", *Acoustical Physics*, Vol. 49 No. 4, pp. 463-74, available at: www.springerlink.com/content/y2752m7ju272l375

Dular, M., Bachert, R., Stoffel, B. and Širok, B. (2007), "Experimental evaluation of numerical simulation of cavitating flow around hydrofoil", *European Journal of Mechanics – B/Fluids*, Vol. 24 No. 4, July-August 2005, pp. 522-38.

Grist E. (1998), *Cavitation and the Centrifugal Pump, A Guide for Pump Users*, Taylor and Francis, London.

Jiang, Y.Y., Yoshimuraa, S., Imaia, R., Katsuraa, H., Yoshidaa, T. and Kato, C. (2007), "Quantitative evaluation of flow-induced structural vibration and noise in turbomachinery by full-scale weakly coupled simulation", *Journal of Fluids and Structures*, Vol. 23, pp. 531-44.

Kim, J.H., Koichi, I., Satoshi, W. and Akinori, F. (2006), "Supression of cavitation surge of impeller inducer by inserting ring – shaped inlet plate", *International Symposium on Cavitation, CAV 2006, Wageningen*.

Kimura, T., Yoshida, Y. and Shimagaki, M. (2006), "Numerical simulation for unsteady cavitating flow in a turbopump inducer", *International Symposium on Cavitation, CAV (2006), Wageningen*.

Langhtjem, M.A. and Olhoff, N. (2004), "A numerical study of flow-induced noise at two-dimensional centrifugal pump. Part 1. Hydrodynamics", *Journal of Fluids and Structures*, Vol. 19, pp. 349-68.

Marjavaara, D. and Lundström, S. (2007), "Response surface-based shape optimisation of a Francis draft tube", *International Journal of Numerical Methods for Heat and Fluid Flow*, Vol. 17 No. 1, pp. 34-45.

Matijašević, B., Guzović, Z. and Martinis, V. (2002), "Imaging the transient boundary layer on a free rotating disc", *Annals of the New York Academy of Sciences*, Vol. 972 No. 1, pp. 67-72.

Matijašević, B., Sviderek, S. and Mihalić, T. (2006), "Effect of turbulence model on unsteady flow simulation in radial fan", *WSEAS Transactions on Fluid Mechanics*, Vol. 1 No. 5, pp. 346-54.

Predin, A. and Biluš, I. (2003), "Influence of additional inlet flow on the prerotation and performance of centrifugal impellers", *Journal of Hydraulic Research*, Vol. 41 No. 2, pp. 207-16.

Wang, J., Priestman, G.H. and Tippetts, J.R. (2006), "Modelling of strongly swirling flows in a complex geometry using unstructured meshes", *International Journal of Numerical Methods for Heat and Fluid Flow*, Vol. 16 No. 8, pp. 910-26.

Further reading

Brennen, C.E. (2007), "A multifrequency instability of cavitating inducers", *Journal of Fluids Engineering*, Vol. 129 No. 6, pp. 731-6.

de Palma, P. (2006), "Numerical simulations of three-dimensional transitional compressible flows in turbomachinery cascades", *International Journal of Numerical Methods for Heat & Fluid Flow*, Vol. 16 No. 4, pp. 509-29.

Lakshminarayana, B. (1996), *Fluid dynamics and heat transfer of Turbomachinery*, John Wiley & Sons Inc., New York, NY.

Corresponding author

Ignacijo Biluš can be contacted at: ignacijo.bilus@uni-mb.si

To purchase reprints of this article please e-mail: **reprints@emeraldinsight.com**
Or visit our web site for further details: **www.emeraldinsight.com/reprints**